PUBLICATIONS OF THE ASTRONOMICAL SOCIETY OF THE PACIFIC, **125**:539–547, 2013 May

Korean VLBI Network Receiver Optics for Simultaneous Multifrequency Observation: Evaluation

SEOG-TAE HAN,[1] JUNG-WON LEE,[1] JIMAN KANG,[1] CHUNG-SIK OH,[1] DO-YOUNG BYUN,[1] DO-HEUNG JE,[1] MOON-HEE CHUNG,[1] SEOG-OH WI,[1] MINKYU SONG,[1] YONG-WOO KANG,[1] SANG-SUNG LEE,[1] SOO-YEON KIM,[2] TETSUO SASAO,[2] PAUL F. GOLDSMITH,[3] AND RICHARD WYLDE[4]

Received 2013 February 21; accepted 2013 April 22; published 2013 May 6

ABSTRACT. We have developed a new millimeter wave receiver system with input optics that support simultaneous observations in four bands of 22, 43, 86, and 129 GHz to facilitate calibrating tropospheric phase fluctuations for millimeter-wave VLBI observations. In order to make simultaneous observations in four bands pointing at the same position in sky, it is crucial that errors among the beams from any misalignments should be kept small. After doing the beam alignment in the laboratory, on-site test observations were carried out so as to evaluate the performance. The result is that the beam centers of the four bands with reference to the 86 GHz beam center were aligned within 2″ over most of the elevation range of the Korean VLBI Network (KVN) 21 m telescope. Measured telescope aperture efficiencies including the multiband receiver optics are 65% at 22 GHz, 62% at 43 GHz, 57% at 86 GHz, and 38% at 129 GHz. Through this novel optics covering wide RF bandwidth effectively, we can simultaneously observe the SiO maser transitions at 43, 86, and 129 GHz and in addition the water maser line at 22 GHz.

1. INTRODUCTION

In recent years, millimeter-wave and submillimeter-wave VLBI (very long baseline interferometry) observations have been widely carried out. Even though various VLBI observations at millimeter wave and submillimeter wavelengths have been successfully performed, phase fluctuations due to tropospheric water vapor remain a key issue in terms of degradation of the sensitivity and imaging capability. For example, the estimated coherence time at 100 GHz with an Allan standard deviation of 10^{-13} is estimated, due to the typical turbulent troposphere, to be as short as 16 s (Sasao 2003). In order to reduce the degradation caused by tropospheric phase fluctuations, both water vapor radiometry and phase referencing techniques have been developed and applied to millimeter and submillimeter VLBI observations.

Reasonable observational results by using water vapor radiometry techniques have been achieved at dry and high-altitude sites such as Owens Valley and Mauna Kea, Hawaii (Woody et al. 2000; Wiedner & Hills 2000). However, the usefulness of these techniques at more humid and low-altitude sites is still questionable.

Phase referencing techniques for millimeter-wave VLBI observations can be categorized by fast antenna switching or frequency switching (Beasley & Conway 1995; Wright 1996; Middelberg et al. 2005), paired/clustered antennas (Asaki et al. 1996, 1998; Rioja et al. 2002; Porcas et al. 2003) and dual-beam antennas (Honma et al. 2003; Jung et al. 2011). Even though these phase referencing techniques are useful and reliable techniques for phase compensation of tropospheric phase fluctuations, their application to millimeter wave VLBI observations has been limited due to the requirement on the separation angle between target and nearby phase calibration reference sources to achieve low residual phase errors. It is noted that a reference source has to be within 1° of target source to maintain coherence above 90% in case of 172 GHz, even under relatively favorable atmospheric conditions (Sasao 2003).

If we could simultaneously observe a source at different observing frequencies, the residual phase errors would be eliminated because tropospheric phase variations arising from the finite switching cycle time or from the actual separation angle between target and reference source would not be present.

In order to solve problems mentioned above for the phase referencing, the Korean VLBI Network (KVN; Han et al. 2008; Lee et al. 2011) employs a unique multifrequency band receiver system that is able to perform simultaneous observations in up to four bands such as 22, 43, 86, and 129 GHz. Phase calibration using a multifrequency bands receiver system is possible because the phase fluctuations from a given amount of water vapor increase linearly with frequency, i.e., the troposphere is nondispersive in terms of its tropospheric phase fluctuation (Asaki et al. 1998). Therefore, the observed phase properties of source at 22 GHz can be used to calibrate the phases of the same source in the higher frequency bands.

[1] Korea Astronomy and Space Science Institute, Daejeon, South Korea; sthan@kasi.re.kr.
[2] School of Electrical Engineering, Korea University, Seoul, South Korea.
[3] Jet Propulsion Laboratory, California Institute of Technology, Pasadena, CA.
[4] Thomas Keating Ltd., UK.

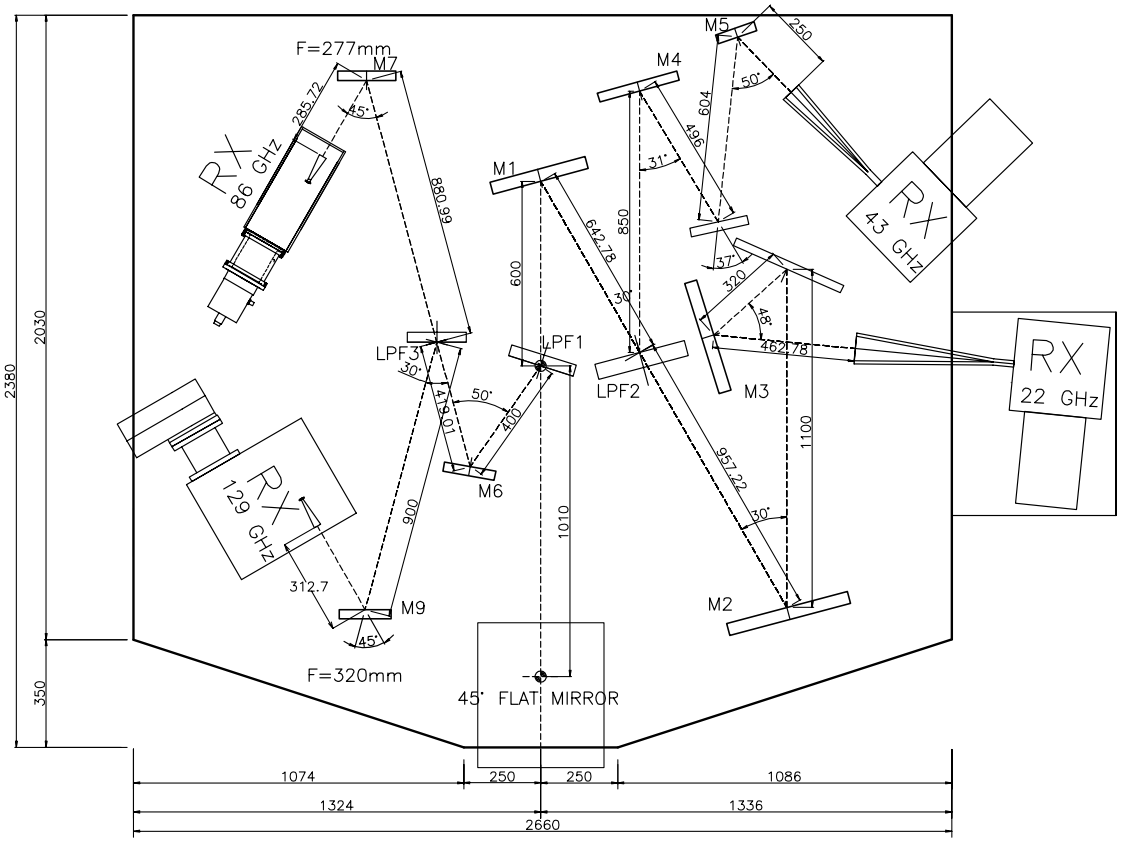

FIG. 1.—Layout of the revised KVN receiver optics. The four receivers are located at the periphery of the quasi-optical frequency selective assembly.

To carry out the simultaneous observations, frequency multiplexing components such as perforated plate filters or frequency selective surface filters are indispensable. Even though several multiband systems employing perforated plate filters have been developed, there is an obvious limitation in terms of wideband performance due to the fact that cylindrical perforations are intrinsically narrowband (Lyons et al. 1990; Moore et al. 1992). The wideband design of the KVN receiver optics is novel in its use of multilayer filters and low-loss mirrors for simultaneous observation. In a previous paper (Han et al. 2008), we dealt with the design of the quasi-optical circuits for the multifrequency receiver system. The test results of the quasi-optical circuit and on-telescope observations are presented in this article.

2. RECEIVER OPTICS

2.1. General Description

The complete receiver optics and receivers installed at the receiver cabins of KVN telescopes are shown in Figures 1 and 2. The beam from the telescope subreflector is first reflected and fed to the following optics by a flat 45° mirror mounted on top of the receiver plate. There are three quasi-optical low-pass filters (LPFs). LPF1 reflects beams of 86 GHz and 129 GHz

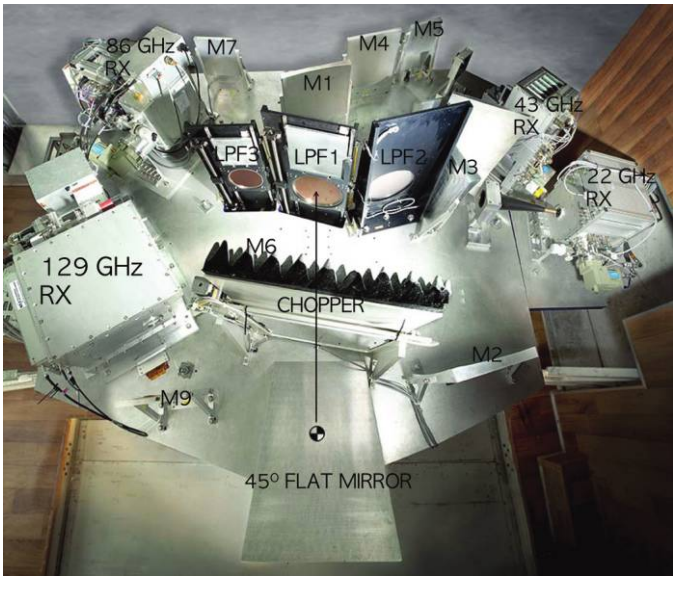

FIG. 2.—View of the complete quasi-optical feed system installed at the receiver cabin of KVN Yonsei telescope. Each LPF is mounted onto a "mode selector", which has a flat mirror and an aperture which function as a filter substitute. A large chopper after the flat 45° mirror inserts an ambient temperature load into the beam path from the secondary in order to calibrate the radiometers.

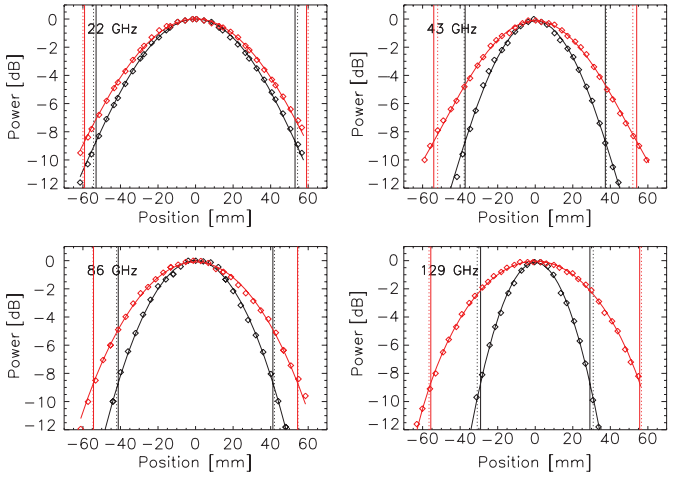

FIG. 3.—Power distribution and beam radius measurements at two different distances from the Cassegrain focus, near (*black*) and far (*red*) (see Table 1 for the measurement locations in each band). The *solid curves* are Gaussians fitted to the measured data. The *dotted vertical lines* indicate the designed beam sizes at the corresponding positions, while the *solid vertical lines* represent measured beam sizes.

bands and transmits the 22 GHz and 43 GHz bands. Similarly, LPF2 passes the 22 GHz band and reflects the 43 GHz band. LPF3 allows the 86 GHz beam to pass while reflecting the 129 GHz beam. Beams are formed by the receiver optics to have −17 dB relative power level at the edge of the subreflector using focusing mirrors designed with the fundamental mode Gaussian beam approximation. Details of the optics were published in Han et al. (2008). Each receiver is equipped with a circular polarizer following a corrugated feed horn. Some feed horns for the lower RF bands (22 GHz, 43 GHz) are mounted outside their respective cryogenic dewars, while the feed horns for the higher bands reside inside their dewars.

2.2. Revised Optics

Frequency-independent beam match was the key objective in the initial design. Since all four feeds have to point the same sky position within the required pointing offset and the required RF bandwidth for each band is a relatively modest 2 GHz, the optics for 86 GHz and 129 GHz bands were modified to have simpler optics by substituting the final mirrors and accompanying flat mirrors before the feeds with a single focusing mirror. This replacement greatly facilitates on-site adjustments during commissioning, as the required tolerances in sky offset are on the order of arcseconds, which translates to submillimeter lateral displacement tolerances for each optical component (see § 3.2). The position and attitude of the 129 GHz receiver were hard to adjust due to the heavier dewar and bulky 4 K cryocooler of this compared to the other receivers.

We have determined that the beam coupling losses over 2 GHz bandwidth caused by the frequency-dependent beams between the revised optics and the feed horns are less than 1%. $M7$ has a focal length of 277 mm with negligible coupling loss with 21.3 mm-diameter, 98 mm long feed horn over the 85–95 GHz range. $M9$ of 320 mm focal length shows a similar match as well to the 21.2 mm diameter, 110 mm long feed horn over the 124–142 GHz frequency range.

TABLE 1

COMPARISON BETWEEN THE DESIGNED AND MEASURED BEAM RADII

Frequency (GHz)	Distance from focus (mm)	Measured beam radius (mm)	Designed beam radius (mm)	Difference (mm)
22	223	53.0 ± 0.4	54.3	1.3
	373	59.1 ± 0.7	60.0	0.9
43	322	37.3 ± 0.3	37.8	0.5
	522	54.0 ± 0.3	52.0	2.1
86	462	41.2 ± 1.1	42.1	0.9
	612	54.4 ± 1.5	54.6	0.2
129	340	29.1 ± 0.3	30.9	1.8
	640	55.6 ± 0.8	56.6	1.0

NOTE.—Due to mechanical interference with mirror mounts, each band has a different measurement plane.

3. LAB ALIGNMENT AND TESTS

3.1. Brief Descriptions of Low-Pass Filters

To make simultaneous observations of four bands possible, the three LPFs work as frequency dividers that route the signal from the subreflector to the appropriate receiver. These filters reflect signals in their stop-band and transmit signals in their pass-band, in a manner similar to normal microwave filters. The essential difference is they work quasi-optically. For optimal performance, incidence angles of the beam at a filter need to be restricted to less than 20°: the incidence angles in our design are 17° and 15° (Han et al. 2008). Filters should be positioned near a beam waist to minimize the filter size. Simulated transmission and reflection losses for each filter were described in Han et al. (2008). About 7% loss in reflection and transmission at each filter were predicted, and actual measurements showed slightly higher degradation, possibly by other misalignments of the optics (see § 3.3). Since the quasi-optical LPFs typically consist of multiple layers with air or dielectric gaps between successive inductive and capacitive layers, we checked where their actual reflection surfaces are located. The effective reflection surfaces of LPF1 and LPF3 are located on the outer surface of each filter. On the other hand, LPF2 is covered with 1.2 mm thick Teflon layer, beneath which reflection was found to occur.

3.2. Beam Alignment

To align the beams, we did iterative alignment in the lab and final adjustment was usually done on the telescope during observations of planets or strong maser sources. Even though we employed a computerized three-axis beam measurement

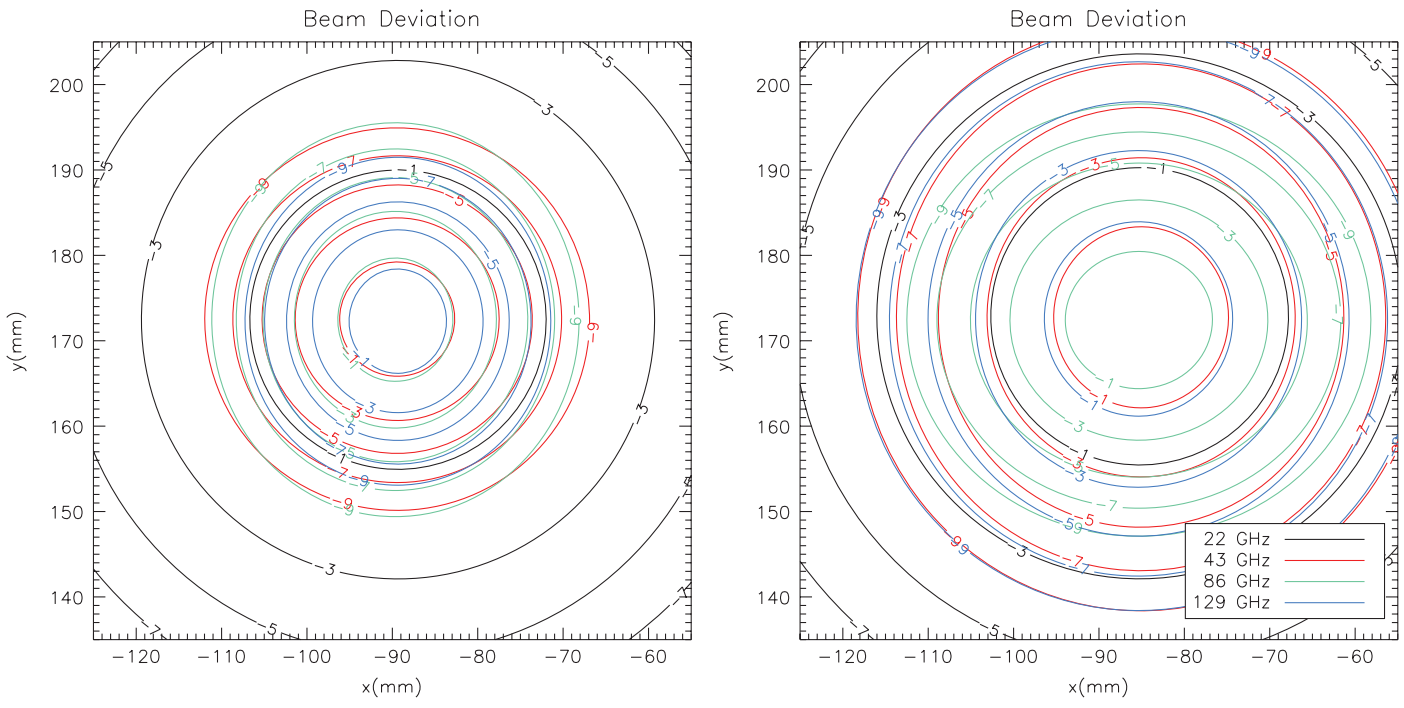

FIG. 4.—Best smoothed fits to power pattern contours of four beams. Note that the measurement plane for the right plot is farther from the Cassegrain focus by 200 mm than the plane for the left plot. Refer to Table 2 for details of the beam centers. Accuracy of the beam measurement system is about 500 microns.

system, the alignment program was quite time-consuming, as four separate bands needed to be adjusted to meet alignment tolerances. A dual-beam laser helped rough alignment between any successive two optical components, while the alignment became more difficult for higher number of optical components. The primary requirement for the alignment work was that each beam be aligned to within 10% of smallest 3 dB beam width (2″ at 129 GHz) on the sky relative to a reference beam direction (86 GHz beam center). The second requirement is to synthesize feed beams conforming to the required edge taper at the subreflector.

We compared the Gaussian beam radius ($1/e$ radius of the electric field amplitude distribution) at the Cassegrain focus as shown in Figure 1 to verify that the receiver optics correctly forms beams of the required edge taper at the subreflector. Figure 3 shows cuts through the beams of the four bands at the indicated distances from the focus. The corresponding beam parameters are listed in Table 1. Designed and measured beam radii differ by less than 2 mm. Therefore, the edge taper is expected to be quite close to 17 dB, the design value (Chapman 2005).

The beam patterns of four frequencies in Figure 4 show circular-shaped beam patterns. This means that the alignment of quasi-optical components among the four bands is correct. The lateral and angular offsets among the beams after laboratory alignment are listed in Table 2, and are within 1 mm and 11′. These results guarantee that any relative pointing offsets and

TABLE 2

BEAM CENTER DEVIATION

Frequency (GHz)	Δx (mm)	Δy (mm)	$(\Delta x^2 + \Delta y^2)^{0.5}$ (mm)	Angle deviation (arcmin)
22	-0.57 ± 0.03	0.30 ± 0.03	0.65 ± 0.03	7.35 ± 1.76
43	-0.32 ± 0.05	0.16 ± 0.06	0.36 ± 0.05	4.07 ± 3.00
129	-0.80 ± 0.03	0.07 ± 0.03	0.81 ± 0.03	9.17 ± 1.81

NOTE.—Measured at a distance of 200 mm displacement from the Cassegrain focus (toward the secondary). All offsets are referred to the beam center at 86 GHz.

TABLE 3

MEASURED LOSSES OF LPF1 AND LPF2 IN THE 22/43 GHz BANDS

	LPF1		LPF2		LPF1+LPF2	
Frequency (GHz)	LCP (%)	RCP (%)	LCP (%)	RCP (%)	LCP (%)	RCP (%)
21.5	0.70	1.16	2.48	3.11	3.15	4.20
22	0.80	0.80	2.53	2.57	3.30	3.32
23	0.47	0.46	2.63	2.57	3.07	3.01
42.36	1.08	1.08	3.02	5.38	4.03	6.35
43.11	1.29	0.88	3.01	2.90	4.23	3.74
43.86	1.48	1.15	1.82	1.82	3.24	2.93

NOTE.—Uncertainty in each loss estimate is no greater than ± 1.4. Both LPF1 and LPF2 give transmission losses in the 22 GHz band. However, LPF1 gives transmission loss while LPF2 gives reflection loss in the 43 GHz band. The data are excerpted from Lee et al. (2011) for completeness.

TABLE 4

MEASURED LOSSES OF LPF1 AND LPF3 IN THE 86/129 GHz BANDS

Frequency (GHz)	LPF1+flat mirror[a] LCP (%)	LPF1+flat mirror[a] RCP (%)	Flat mirror+LPF3 LCP (%)	Flat mirror+LPF3 RCP (%)	LPF1+LPF3 LCP (%)	LPF1+LPF3 RCP (%)
86	5.1	5.9	4.1	4.0	8.3	9.6
90	7.3	8.2	4.7	4.7	11.4	12.7
94	7.5	8.8	6.0	6.4	13.2	14.9
129	4.7	5.3	1.7	1.7	5.3	5.6
134	6.5	6.3	1.6	1.8	6.5	6.6
138	7.3	7.2	1.7	1.5	7.7	7.9
142	8.7	8.9	1.9	1.5	10.4	10.6

NOTE.—Uncertainty in each loss estimate is no greater than ±1.3. LPF1 has reflection losses in both bands, while LPF3 produces transmission loss in the 86 GHz band and reflection loss in the 129 GHz band.

[a] Only applicable for 129 GHz band: no flat mirror for 86 GHz band.

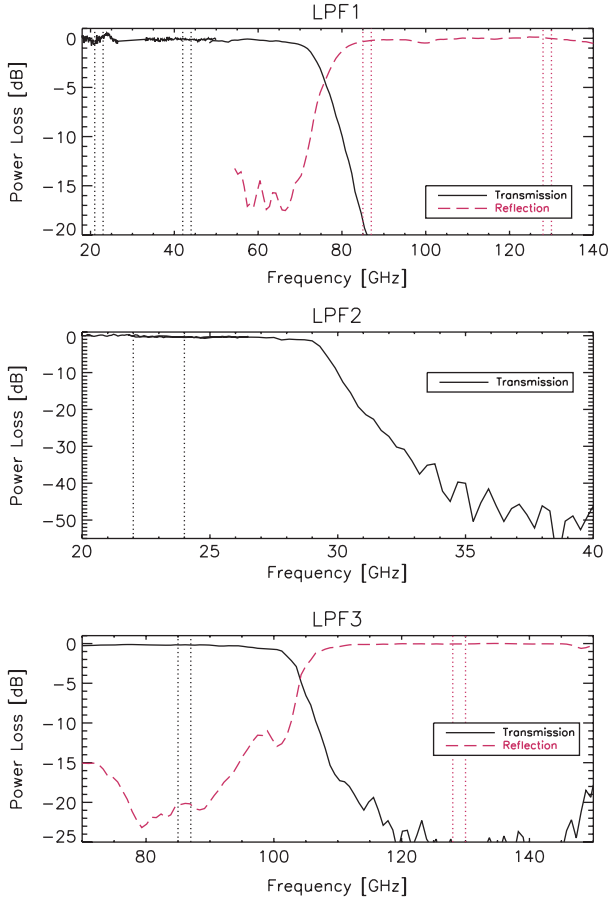

FIG. 5.—Wideband FTS measurement data for KVN LPFs (data courtesy of QMC Instruments, Cardiff, UK). For 43/129 GHz bands, the relevant LPFs are used in reflection. The 22 GHz beam passes through LPF1 and LPF2, as does the 86 GHz beam through LPF1 and LPF3. The *dotted vertical lines* mark the required RF bandwidth of each KVN band.

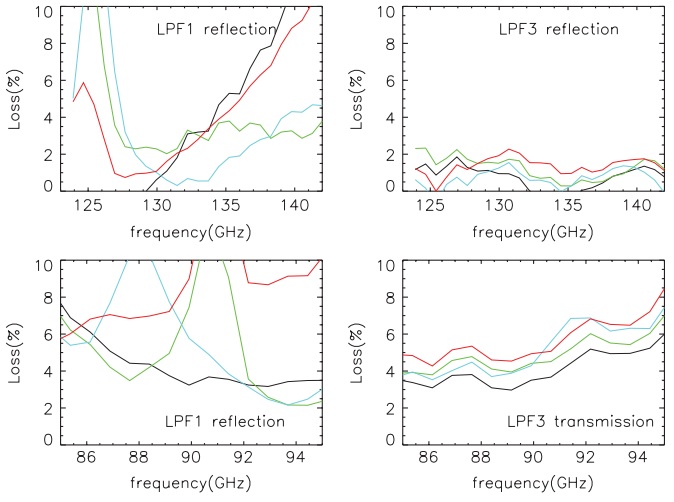

FIG. 6.—Zoomed FTS-measured losses of the LPF1 and LPF3 in 86/129 GHz bands. The four curves in each plot represent performance of the filters of different serial numbers.

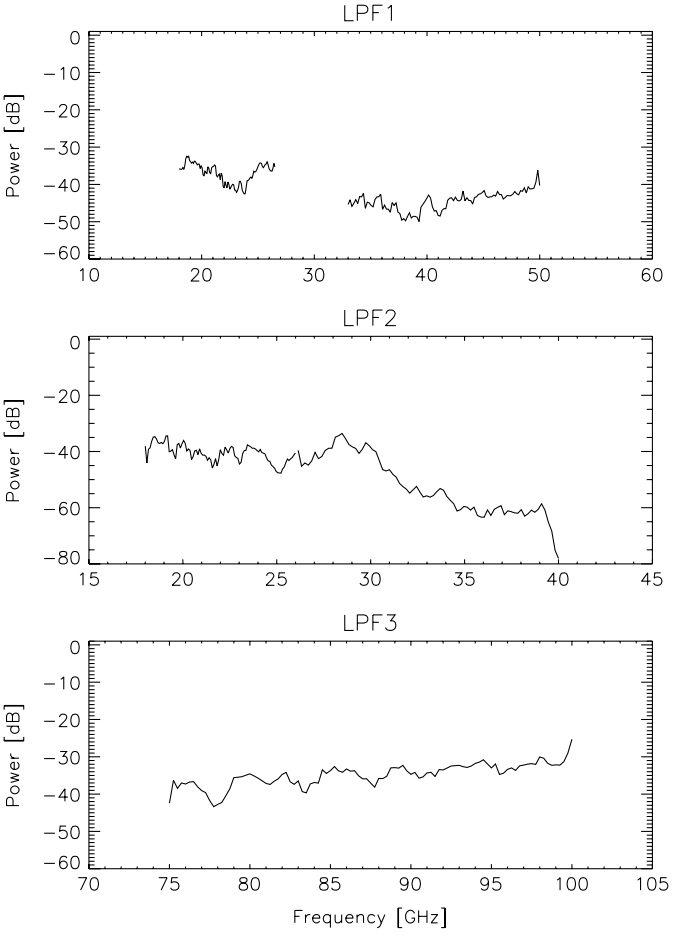

FIG. 7.—Cross polarization losses for LPF2 and LPF3. The cross polarization data for LPF1 in the 129 GHz band are missing as a proper signal source was not available leading to poor S/N ratio in the data.

TABLE 5
BEAM ALIGNMENTS OF THE 22/43/129 GHZ BANDS

	22 GHz		43 GHz		129 GHz	
	Offset (Az) (arcsec)	Offset (El) (arcsec)	Offset (Az) (arcsec)	Offset (El) (arcsec)	Offset (Az) (arcsec)	Offset (El) (arcsec)
Before	>5	>5	>5	>5	>5	>5
After	-3.1 ± 0.7	$+3.1 \pm 0.7$	$+1.7 \pm 0.1$	$+2.0 \pm 0.3$	$+0.8 \pm 0.4$	-0.9 ± 0.5

NOTE.—With respect to the center of the 86 GHz beam on the KVN Yonsei telescope.

efficiency degradation are not severe. The fact the beam offsets on the sky must be less than 2″ usually demanded more accurate adjustments during final installation of the receiver optics on the telescope.

3.3. Insertion Loss of Optics

Except for the 129 GHz band receiver, which has four superconducting mixers for dual polarized sideband rejection operation, high electron mobility transistor (HEMT) low-noise amplifiers (LNAs) are used in the other receivers. The 22, 43, and 129 GHz band receivers were built in house, and the 86 GHz band receiver was developed by collaboration with the Five College Radio Astronomy Observatory (University of Massachusetts, Amherst, MA). All frontend receivers support dual circular-polarization observation and show competitive noise temperatures excluding the input optics: 40 K for 22 GHz, 70 K for 43 GHz, 60 K for 86 GHz, and <80 K (SSB) for the 129 GHz receivers. Using the hot/cold load technique, we measured the increase of noise temperature due to dissipation and spillover loss of the intervening optics in each receiver band. Measured optics losses including LPF1 and LPF2 for 22 GHz and 43 GHz bands are about 3–4%, as shown in Table 3. The measured optics losses including LPF1 and LPF3 for the 86 GHz and 129 GHz bands are shown in Table 4. For comparison, wideband Fourier transform spectrometer data offered by the filter manufacturer are shown in Figures 5 and 6. The loss of LPF3 in transmission is 2–3 times higher than loss in reflection. Particularly since LPF1 was engineered to have low loss over the VLBI bandwidths 84–86 GHz and 128–130 GHz, those filters show significantly higher measured loss at other frequencies. Note that filter configurations such as LPF1+flat mirror and flat mirror+LPF3 contain possible spillover losses produced by misalignment of flat mirrors, which are attached to the mode selector to the remaining optics. This spillover loss was measured and estimated to be about 1% to 2% for the 86 GHz and 129 GHz bands.

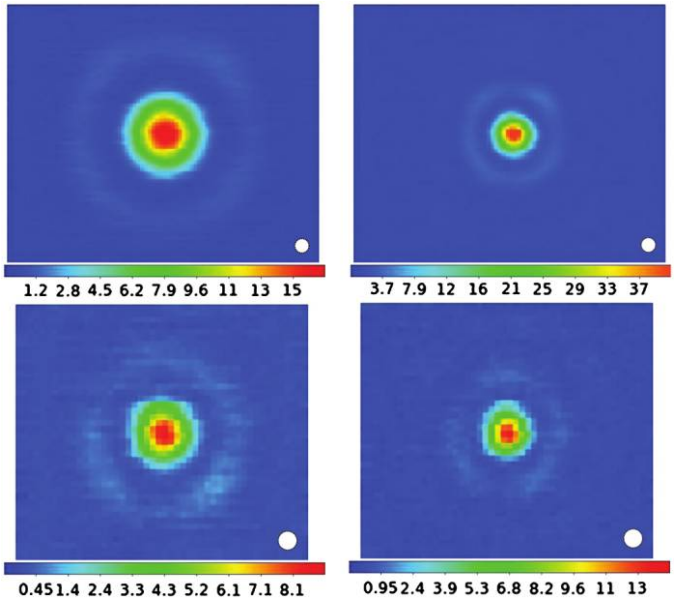

FIG. 8.—Maps of Venus at 22 GHz (*upper left*) and 43 GHz (*upper right*). The map size is $12' \times 10'$; Maps of Mars at 86 GHz (*lower left*) and 129 GHz (*lower right*). The map size is $3.5' \times 3'$. The sizes of the planets are shown as *white circles* in the corners of the maps.

3.4. Cross Polarization Properties of LPFs

For VLBI observations employing circular polarization, good cross-polarization performance of the quasi-optical components is crucial. The cross-polarization properties of an ellipsoidal mirror and a corrugated feed horn are well known. However, cross-polarization properties of the quasi-optical filter used in this feed system have not been well studied so far. To assess cross polarization of the filters we measured their cross polarization using a linear polarized CW signal. The measured

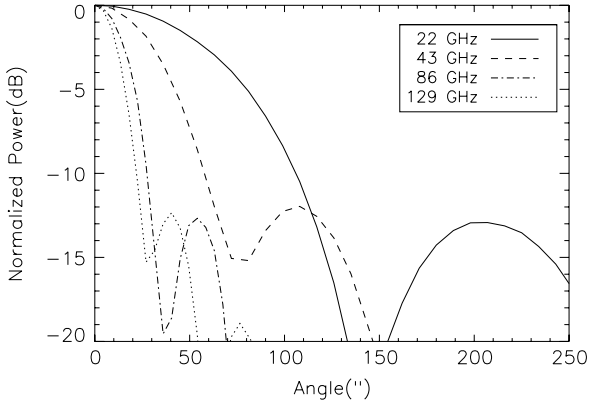

FIG. 9.—Azimuthally averaged beam patterns at 22, 43, 86, and 129 GHz.

TABLE 6
BEAM SIZES AND FIRST SIDELOBE LEVELS OF KVN YONSEI TELESCOPE

Frequency (GHz)	Obs. date	Source name	Elevation (degree)	Source size (arcsec)	Beam size (arcsec)	First sidelobe level (dB)
22.235	2012 Apr 27	Venus	70	35.5	125	−12.9
43.122	2012 Apr 27	Venus	70	35.5	63	−12.0
86.243	2012 Mar 12	Mars	42	13.8	33	−12.6
129.363	2012 Mar 12	Mars	42	13.8	23	−12.6

results, shown in Figure 7, reveal that their losses are less than 30 dB as desired.

4. ON-SITE TEST RESULTS

4.1. Alignment Among 22/43/86/129 GHz Beams

It is crucial to align the beams of the KVN receiver system because poor beam alignment leads to large loss of flux measurements during simultaneous multifrequency observations of point sources. Therefore, as stated previously, we aimed to align the beams to within less than 10% of the FWHM of the smallest beam (e.g., 2″ at 129 GHz) to limit the expected flux losses to be less than 2.5%. This coalignment facilitates pointing for higher frequencies in that pointing offsets measured in the lower frequency benefited from both stronger sources and lower system noise can be applied for higher frequency observation. The first beam alignment measurement of KVN Yonsei telescope started in March 2011 after installing the receiver system including the quasi-optical feed system. The test observations for the antenna beam pattern and aperture efficiency were subsequently performed. We carried out cross scans of Mars at 22, 43, 86, and 129 GHz. The beam alignment was carried out by measuring the relative pointing offsets of each frequency using the 86 GHz beam as reference. If the relative pointing offset was larger than the requirement, we readjusted the flat mirrors and feed horns associated with the receiving band to reach the relative pointing offset requirement. Table 5 shows the results of the beam alignments with respect to the 86 GHz beam. The beams at each frequency were aligned well in both azimuth and elevation after the in situ readjustments.

4.2. Antenna Beam Patterns

Figure 8 shows the maps of Mars at 86 GHz and 129 GHz (obtained simultaneously) and also Venus at 22 GHz and at 43 GHz. The beam patterns have been averaged azimuthally and radial profiles are shown in Figure 9. Beam widths and sidelobe levels are estimated from the obtained radial profiles. Table 6 summarizes the observed parameters and their values. The angular sizes of Mars and Venus were included to estimate the main beam sizes from the observed patterns.

Measured beam sizes at 22, 43, and 86 GHz are 5% to 8% smaller than the beam size of a uniformly illuminated circular aperture. The first sidelobe levels at 97 GHz of about −13 dB are similar to the value obtained during observations for antenna acceptance (Kim et al. 2011). For the earlier measurements, only one flat mirror with a feed horn was used to verify antenna performance so we conclude that the quasi-optics does not produce any degradation of the beam quality. The beam sizes and the first sidelobe levels at 22 GHz and 43 GHz are almost the same as the values reported by Lee et al. (2011).

4.3. Aperture Efficiency

We estimated the aperture efficiencies at four frequency bands from the cross scan results of the planets using the equations (1)–(4) of Lee et al. (2011). In order to estimate receiver gains, we used the hot and cold loads; i.e., an absorber in ambient temperature and an absorber immersed in liquid nitrogen. Attenuation in the atmosphere at each frequency is corrected by measuring optical depth using the conventional sky dipping method. Table 7 summarizes the estimated aperture efficiencies with the corresponding measurement conditions. The obtained efficiencies of 48% and 30% at 86 GHz and 129 GHz are

TABLE 7
APERTURE EFFICIENCIES OF KVN YONSEI TELESCOPE

Frequency (GHz)	Obs. date	Source name	Elevation (deg)	Source size (arcsec)	Brightness temperature (K)	Aperture efficiency (%)
22.235	2012 Oct 25	Jupiter	30–60	46.1	134 ± 4 (P03)	65 ± 1
43.122	2012 Oct 25	Jupiter	30–60	46.1	150 ± 15 (G94)	62 ± 2
86.243	2012 Oct 25	Venus	30–60	13.7	357.5 ± 13 (U80)	57 ± 2
129.363	2012 Oct 25	Venus	30–60	13.7	331 (F92)	38 ± 3

NOTE. —Errors of aperture efficiencies are 1σ, not including systematic errors arising from uncertainties in the brightness temperatures.
References.—(F92) Fahd 1992; (G94) Greve et al. 1994; (P03) Page et al. 2003; (U80) Ulich et al. 1980.

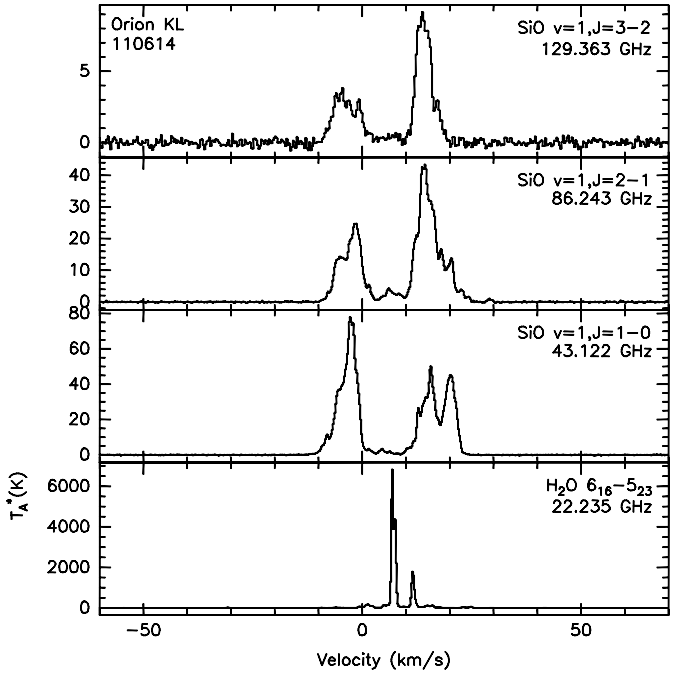

FIG. 10.—Simultaneous four-bands observation of strong maser lines toward Orion-KL.

significantly lower than the expected values from the measured antenna surface accuracy of 150 μm rms (Kim et al. 2011) with which the aperture efficiencies at 100 GHz and 129 GHz is expected to be approximately 55% and 44%, respectively. This implies that there may be significant beam coupling loss between the antenna optics and the receiver quasi-optics. In order to improve aperture efficiency, we have adjusted the receiver plate position of the KVN Yonsei station, about 150 mm off, closer to the subreflector where best efficiencies were obtained at 97 GHz in the past antenna acceptance test. Aperture efficiencies for 86 GHz and 129 GHz band eventually get improved to 57% at 86 GHz and 38% at 129 GHz, similarly to the expected values. This improvement makes certain that the receiver optics are properly designed and implemented.

4.4. An Example of Astronomical Observations

The four-band system of KVN covers many interesting line and continuum spectra in radio astronomy. For example, the H_2O and CH_3OH maser lines at 22 GHz band, and the SiO, CH_3OH maser lines can be observed at 43/86/129 GHz band. The radio continuum sources are also candidates at each band. We have carried out simultaneous multifrequency observations to test the four-band system with H_2O and SiO maser lines. We chose the well-known star-forming region Orion-KL as a test object. Figure 10 shows the results of simultaneous four-band observation.

5. SUMMARY

We have developed a new millimeter wave receiver system that can perform simultaneous observations in up to four well-separated frequency ranges including 22, 43, 86, and 129 GHz bands to calibrate tropospheric phase fluctuation for the millimeter wave VLBI observations.

1. We have successfully obtained simultaneous spectral lines toward Orion-KL in all four bands, which is to our knowledge the first time that three SiO maser transitions (at 43, 86, and 129 GHz) and a water maser at 22 GHz have been observed simultaneously.

2. The designed beam radius was compared with the measurements near the telescope's Cassegrain focus enabling us to conclude that the components of the quasi-optical feed system have been properly designed, fabricated, and aligned.

3. In order to assess optics losses, Y-factor measurements were carried out in front of the Cassegrain focus. Measured losses are $<3.5\%$ at 22 GHz, $<4.5\%$ at 43 GHz, $<12.5\%$ at 86 GHz, and $<7.5\%$ at 129 GHz . Most of the loss is attributed to dissipation in the LPFs with an additional contribution by spillover within the quasi-optical system.

4. Alignment of the beams on the sky showed peak offsets within 2″; a level that is less than 10% of the expected beam width of the highest-frequency 129 GHz band.

5. Telescope aperture efficiencies including the receiver optics are 65% at 22 GHz, 62% at 43 GHz, 57% at 86 GHz, and 38% at 129 GHz.

REFERENCES

Asaki, Y., Saito, M., Kawabe, R., Morita, K., & Sasao, T. 1996, Radio Sci., 31, 1615
Asaki, Y., Shibata, K. M., Kawabe, R., Roh, D.-G, Saito, M., Morita, K., & Sasao, T. 1998, Radio Sci., 33, 1297
Beasley, A. J., & Conway, J. E. 1995, in ASP Conf. Ser. 82, Very Long Baseline Interferometry and the VLBA, ed. J. A., Zensus, et al. (San Francisco: ASP), 327
Chapman, E. 2005, Antedo Technical Memo, KVN-21-TM-130 (San Jose: Antedo, Inc.)
Fahd, A. K. 1992, NASA Technical Report No. 1992-1 (Washington: NASA)
Greve, A., Steppe, H., Graham, D., & Schalinski, C. J. 1994, A&A, 286, 654
Han, S.-T., Lee, J.-W., Kang, J. M., Je, D.-H., Chung, M.-H., Wi, S.-O., Sasao, T., & Wylde, R. 2008, Int. J. Infrared Millimeter Waves, 29, 69
Honma, M., et al. 2003, PASJ, 55, 157
Jung, T., et al. 2011, PASJ, 63, 375
Kim, K.-T., Byun, D.-Y., Je, D.-H., Wi, S.-O., Bae, J.-H., Jung, T.-H., Lee, C.-H., Han, S.-T., et al. 2011, JKAS, 44, 81
Lee, S.-S., et al. 2011, PASP, 123, 1398
Lyons, B. N., et al. 1990, Microwave J., 6, 197

Middelberg, E., Roy, A. L., Walker, R. C., & Falcke, H. 2005, A&A, 433, 897
Moore, E. L., et al. 1992, Microwave J., 10, 72
Page, L., Barnes, C., Hinshaw, G., Spergel, D. N., Weiland, J. L., Wollack, E., Bennett, C. L., Halpern, M., et al. 2003, ApJS, 148, 39
Porcas, R. W., et al. 2003, in ASP Conf. Ser., 306, New Technologies in VLBI, ed. Y. C., Minh (San Francisco: ASP), 39
Rioja, M.-J., Porcas, R. W., Desmurs, J.-F., Alet, W., Guruits, L. I., & Schilizzi, R. T. 2002, in Proc. 6th European VLBI Network Symposium, ed. E. Ros, et al. (Bonn: Max-Plank-Institut für Radioastronomie) 57
Sasao, T. 2003, in ASP Conf. Ser., 306, New Technologies in VLBI, ed. Y. C. Minh (San Francisco: ASP), 53
Ulich, B. L., Davis, J. H., Rhodes, P. J., & Hollis, J. M. 1980, IEEE Trans. Antennas Propag., , AP-28, 367
Wiedner, M. C., & Hills, R. E. 2000, in ASP Conf. Ser. 217, Imaging at Radio through Submillimeter Wavelengths, ed. J. G. Mangum, & S. J. E. Radford, (San Francisco: ASP), 327
Woody, D., Carpenter, J., & Scoville, N. 2000, in ASP Conf. Ser., 217, Imaging at Radio through Submillimeter Wavelengths, ed. J. G. Mangum, & S. J. E. Radford, (San Francisco: ASP), 317
Wright, M. C. H. 1996, PASP, 108, 520